JACS
JOURNAL OF THE AMERICAN CHEMICAL SOCIETY

Article

pubs.acs.org/JACS

State-to-State Mode Specificity: Energy Sequestration and Flow Gated by Transition State

Bin Zhao,[†] Zhigang Sun,[‡] and Hua Guo*[,†]

[†]Department of Chemistry and Chemical Biology, University of New Mexico, Albuquerque, New Mexico 87131, United States

[‡]State Key Laboratory of Molecular Reaction Dynamics and Center for Theoretical and Computational Chemistry, Dalian Institute of Chemical Physics, Chinese Academy of Sciences, Dalian 116023, China

Supporting Information

ABSTRACT: Energy flow and sequestration at the state-to-state level are investigated for a prototypical four-atom reaction, $H_2 + OH \rightarrow H + H_2O$, using a transition-state wave packet (TSWP) method. The product state distribution is found to depend strongly on the reactant vibrational excitation, indicating mode specificity at the state-to-state level. From a local-mode perspective, it is shown that the vibrational excitation of the H_2O product derives from two different sources, one attributable to the energy flow along the reaction coordinate into the newly formed OH bond and the other due to the sequestration of the vibrational energy in the OH spectator moiety during the reaction. The analysis provided a unified interpretation of some seemingly contradicting experimental observations. It is further shown that the transfer of vibrational energy from the OH reactant to H_2O product is gated by the transition state, accomplished coherently by multiple TSWPs with the corresponding OH vibrational excitation.

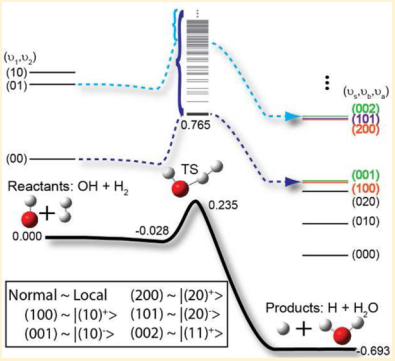

INTRODUCTION

The concept of the transition state occupies a central place in our understanding of chemical reactions. Its paramount importance in chemical rate theory as a bottleneck for reactive flux is well established.[1,2] Yet, its role in regulating energy flow in state-to-state reaction dynamics is still not fully appreciated.[3] This latter issue is akin to the much discussed mode specificity in chemical reactions,[4−7] in which various reactant modes might have different efficacies in promoting the reaction. Such non-statistical phenomena underscore the dynamical nature of many activated bimolecular reactions. A better understanding of these issues helps to attain a deeper understanding of many important chemical processes in gaseous environments such as combustion, atmospheric chemistry, and interstellar chemistry.

A well-known rule of thumb for mode specificity is that of Polanyi,[8] who pointed out that for atom−diatom systems, translational energy promotes early-barrier reactions, while vibrational energy enhances late-barrier ones. The general success of Polanyi's rules clearly underscores the importance of the transition state in controlling the energy flow in such reactions. More recently, we have extended these rules to reactions involving polyatomic molecules by proposing the so-called Sudden Vector Projection (SVP) model.[9,10] Assuming the collision time scale is significantly shorter than that of intramolecular vibrational energy redistribution in the reactant molecules, the SVP model attributes the ability of a reactant mode in promoting the reaction to the projection of its normal-mode vector onto the reaction-coordinate vector at the transition state. Such a projection provides a quantifiable measure of the coupling strength with the reaction coordinate in the sudden limit. Specifically, a large SVP value signifies a strong coupling, thus efficient energy flow into the reaction coordinate and high ability to enhance the reactivity. Invoking the microscopic reversibility, the SVP model also allows the prediction of product energy disposal in the sudden limit. It is important to note that, like Polanyi's rules, the SVP model recognizes the key role of the transition state in mode-specific reaction dynamics. This model has been applied to numerous reactive systems and its predictions have generally been validated.[11]

The sudden nature of many activated gaseous bimolecular reactions has long been recognized, which has led to several Franck−Condon models for characterizing state-to-state reaction dynamics.[12−14] In particular, it has been shown that state-to-state reaction attributes can be obtained approximately by overlapping transition-state wave packets (TSWPs) with asymptotic ones. These approaches share the same spirit as the SVP model, but provide a much more quantitative perspective on the transition-state control of reaction dynamics. Very recently, Manthe and co-workers further proposed an *exact* solution to the state-to-state quantum reactive scattering by propagating TSWPs into both the reactant and product channels.[15,16] This TSWP approach has its genesis in Miller's quantum transition-state theory,[17,18] thus further accentuating the importance of the transition state in regulating reactivity in bimolecular reactions. This TSWP method has been applied to both the $D + H_2$ and $H + CH_4$ reactions with full dimensionality,[14,15,19,20] shedding much light on how the transition state controls the state-to-state dynamics. Our recent

Received: October 31, 2015
Published: November 27, 2015

© 2015 American Chemical Society

DOI: 10.1021/jacs.5b11404
J. Am. Chem. Soc. 2015, 137, 15964−15970

studies using our own implementation of the TSWP approach[21,22] have revealed that reactant modes with large SVP values facilitate energy flow into the reaction coordinate, confirming the predictions of the SVP model.[23,24]

One of the most interesting and surprising observations from these recent TSWP studies is the so-called "loss of memory" effect near the reaction threshold.[20,24] In other words, product state distributions are insensitive to reactant internal excitations. Taking the example of the H/Cl + H_2O → H_2/HCl + OH reactions, our recent quantum scattering calculations have shown that single quantum excitations of the H_2O vibrational modes have essentially no effect on the product internal state distributions near the reaction threshold.[24] Interestingly, there is experimental evidence supporting this observation. In a pioneering study of the H + D_2O → HD + OD reaction, Zare and co-workers found that the OD product is always in its ground vibrational state even when the D_2O reactant is in excited normal-mode states and the OD rotational distribution is independent of the initial excitation of the D_2O reactant.[25] On the other hand, Crim and co-workers have elegantly demonstrated for the H/Cl + H_2O reactions that the OH product is predominated in its v = 0 or 1 state if the H_2O reactant is prepared in the near-degenerate $|04\rangle^-$ or $|13\rangle^-$ local-mode state, respectively,[26,27] suggesting a strong memory effect. In other words, the vibrational energy in the non-reactive OH moiety is preserved, indicating energy sequestration in the OH spectator. A better understanding of these two powerful, but seemingly contradicting viewpoints is thus desired.

The vibrational energy sequestration in reactions or the lack thereof noted in these studies represents an important issue in bimolecular reactions involving larger species. This is because many such reactions often include only a small number of atoms, leaving the majority of modes as spectators.[3] In this publication, we present a detailed full-dimensional quantum dynamical calculations of a prototypical four-atom reaction, H_2 + OH → H + H_2O, with full quantum state resolution of both reactants and products. This reaction has served as a proving ground in understanding the state-to-state quantum dynamics of polyatomic reactions,[22,28−35] which is necessary due to the presence of quantum effects such as zero-point energy and tunneling. This reaction is also of practical importance in both combustion and atmospheric chemistry.[36] These previous studies have firmly established that the OH moiety is a spectator throughout the reaction, but how it sequesters its internal energy has seldom been explored at the state-to-state level.[37,38] In this work, we use the TSWP approach to address mode specificity at the state-to-state level and to understand the origin of the product vibrational excitation. In addition to confirming the spectator nature of the OH moiety, our results further reveal that the energy sequestration in the spectator mode, much like the energy flow from active modes, is also controlled by the transition state.

THEORY

The TSWP method for state-to-state quantum reactive scattering[15,16] is based on the quantum transition-state theory of Miller and co-workers,[17,18] which was initially intended for formulating a direct way to calculate cumulative reaction probabilities and thermal rate constants from flux correlation functions with dividing surfaces located near the transition state. Specifically, Manthe and co-workers extended this formalism to compute the S-matrix elements utilizing generalized flux correlation functions and three dividing surfaces.[15,16] In this TSWP method, the initial wave packets are selected as the eigenstates of a thermal flux operator, which is defined near the transition state as

$$\hat{F}_T = e^{-\hat{H}/2k_BT}\,\hat{F}\,e^{-\hat{H}/2k_BT} \tag{1}$$

where k_B is the Boltzmann constant, T the reference temperature, and $\hat{F} = i[\hat{H},h(q)]$ the flux operator with h as the Heaviside step function that defines the dividing surface near the transition state. The temperature is introduced because the Boltzmann operators in $\hat{F}_T$ improve the numerical stability in calculating the thermal flux eigenstates.

The thermal flux operator can be expressed in its eigenstate representation,[39]

$$\hat{F}_T = \sum_n f_T^n\,|f_T^n\rangle\,\langle f_T^n| \tag{2}$$

Its eigenvalues and eigenstates come in pairs, in which the eigenvalues f_T^n have the same absolute value but opposite signs,[40] and the corresponding eigenstates $|f_T^n\rangle$ are complex conjugates of each other. These eigenpairs can be interpreted as the ro-vibrational wave functions of the activated complex in the transition-state region, and their contributions to the reactivity can be readily analyzed.[19]

The initial TSWPs are then propagated independently into both the reactant and product arrangement channels and the reactive S-matrix elements are finally assembled as follows,[15]

$$S_{v_p j_p \leftarrow v_r j_r}(E) = \frac{e^{E/k_BT}}{2\pi\eta^{+*}_{v_p j_p}(E)\eta^{-}_{v_r j_r}(E)} \sum_n f_T^n A_{v_p j_p \leftarrow n}(E) A^*_{n \leftarrow v_r j_r}(E) \tag{3}$$

where the energy-resolved projection amplitudes in the product (p) and reactant (r) channels, $A_{v_p j_p \leftarrow n}(E)$ and $A^*_{n \leftarrow v_r j_r}(E)$, are given as Fourier transforms of the appropriate cross-correlation functions:

$$\begin{aligned} A_{v_p j_p \leftarrow n}(E) &= \int_{-\infty}^{\infty} dt\; e^{iEt} C_{v_p j_p \leftarrow n}(t) \\ &= \int_{-\infty}^{\infty} dt\; e^{iEt} \langle \Phi^+_{v_p j_p} | e^{-i\hat{H}t} | f_T^n \rangle \end{aligned} \tag{4a}$$

$$\begin{aligned} A^*_{n \leftarrow v_r j_r}(E) &= \int_{-\infty}^{\infty} dt\; e^{-iEt} C^*_{n \leftarrow v_r j_r}(t) \\ &= \int_{-\infty}^{\infty} dt\; e^{-iEt} \langle f_T^n | e^{i\hat{H}t} | \Phi^-_{v_r j_r} \rangle \end{aligned} \tag{4b}$$

where $\eta^+_{v_p j_p}(E)$ and $\eta^-_{v_r j_r}(E)$ are the energy-normalizing factors of the asymptotic wave functions $|\Phi^+_{v_p j_p}\rangle$and $|\Phi^-_{v_r j_r}\rangle$ for the two channels. They are defined on dividing surfaces in the two asymptotic regions and can be conveniently written as the product of a delta function of the appropriate scattering coordinate and the reactant or product internal state wave functions. Finally, the state-to-state reaction probability $P_{v_p j_p \leftarrow v_r j_r}(E)$ is obtained by taking the square of the corresponding S-matrix element. Only J = 0 results are presented here, but the conclusion should be extendable to other partial waves.

The details of the discretization and propagation are given in our previous publications[22−24] and also in the Supporting Information. The potential energy surface used in the calculations is that of Zhang and co-workers.[41] Careful tests of convergence were carried out.

RESULTS AND DISCUSSION

In Figure 1, the initial state-selected total reaction probabilities (J = 0) as a function of collision energy (E_c) are shown for multiple initial ro-vibrational states of OH with H_2 always in its ground ro-vibrational state. It is clear that the excitation of the OH vibration has little effect on the reactivity. The total reaction probabilities from the vibrationally excited OH reactant are almost the same as the corresponding ones from vibrationally unexcited OH. These observations confirm the spectator character of OH molecule in the reaction. We also note in passing that the rotational excitation of OH inhibits the reaction, consistent with previous theoretical results.[42,43]

DOI: 10.1021/jacs.5b11404
J. Am. Chem. Soc. 2015, 137, 15964−15970

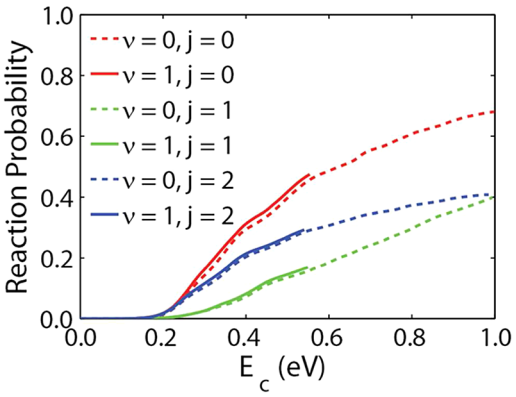

Figure 1. Initial state-selected total reaction probabilities of the reaction $H_2(v = 0, j = 0) + OH(v = 0,1, j = 0,1,2) \rightarrow H + H_2O$ as a function of collision energy.

The SVP model can be used to rationalize the observed spectator nature of the non-reactive OH mode. As discussed above, a reactant mode with a large projection on to the reaction coordinate at the transition state is expected to enhance reaction because the alignment of the two vectors implies facile energy flow from the reactant mode to the reaction coordinate. On the other hand, a small SVP value suggests that such energy flow is likely inefficient, because the reactant vector is poorly aligned with the reaction coordinate. In Table 1, the SVP values for both the reactant and product

Table 1. SVP Values for $H_2 + OH \rightarrow H + H_2O$ Reaction

$H_2 + OH$		$H + H_2O$	
mode	SVP	mode	SVP
H_2	0.36	ν_s	0.66
OH	0.0005	ν_a	0.66
		ν_b	0.15

modes are listed.[10] It is clear from the table that the vibrational mode of the OH reactant has an extremely small SVP value, which suggests near null ability for this mode to enhance the reaction, consistent with its spectator nature.

Let us now examine the spectator nature of the OH moiety from the state-to-state perspective. If the OH mode is indeed a spectator during the reaction, as predicted by the SVP model and implicated in both experiments and calculations, energy deposited into this mode should be well sequestered during the reaction, and eventually deposited into the corresponding product vibrational modes. This is indeed the case, as shown in Figure 2, in which the H_2O product internal state distributions are shown for both the ground and vibrationally excited states of the reactant $OH(v = 0,1)$. The threshold of various H_2O vibrational eigenstates, denoted respectively by the normal-mode quantum numbers in the symmetric stretching, bending, and anti-symmetric stretching modes of $H_2O(\nu_s\nu_b\nu_a)$, are marked in the figure by arrows. It is clear from the figure that there are significant vibrational as well as rotational excitations in the H_2O product for both the $v = 0,1$ states of the OH reactant.

To establish a reference point against which the OH vibrational energy sequestration can be analyzed, we first discuss the H_2O product state distributions for the reaction from the ground state OH reactant, as shown in the left column of Figure 2. For example, at the total energy of 1.2 eV, shown in Figure 2a, the H_2O product is dominated by one and two quanta of symmetric and anti-symmetric stretching excitations, i.e., (100), (001), (200), (101), and (002). As the energy increases to 1.5 eV, shown in Figure 2c, the triply excited stretching states, (300), (201), (102), and (003), are also produced. According to the SVP model,[9,10] the excitation in the stretching modes of the H_2O product can be attributed to their strong coupling with the reaction coordinate at the transition state, as shown in Table 1, indicating facile energy flow from the reaction coordinate into these product modes. These vibrational state distributions thus serve as a baseline in understanding the vibrational energy sequestration for the excited non-reactive OH moiety.

In Figure 2b,d, where the final H_2O ro-vibrational state distributions from the reaction with the OH reactant in its first excited vibrational state are shown, it is clear that the H_2O product internal energy contents are quite different from those shown in the left panels. At the same total energies, the reaction with the vibrationally excited OH reactant produces few H_2O products in the ground and first excited stretching vibrational states. However, the higher stretching states with two and three quanta are disproportionally populated. In contrast to the "loss of memory" effect mentioned above,[19,23] there is a strong correlation between the OH reactant vibrational excitation and the H_2O product vibrational state distribution. We call this *state-to-state mode specificity*.

It might be interesting to further compare the ro-vibrational state distributions of the H_2O product at the same collision energy for both the ground and first excited OH reactants, as shown in Figure 2e,f. Here, the collision energy is related to total energy by $E_t = E_c + E_v$, where E_v is the internal energy of the reactants. The distribution in Figure 2f appears to be shifted by one quantum when compared with that in Figure 2e. This clearly suggests that it may be possible to decompose the H_2O stretching excitations into two parts. First, the strong coupling of these product vibrational modes with the reaction coordinate at the transition state is responsible for at least one quantum excitation in the H_2O stretching modes. Second, the sequestered vibrational energy in $OH(v = 1)$ adds one more quantum to the H_2O product stretching excitation. Similar state-to-state mode specificity has been observed in our earlier work, albeit with quasi-classical trajectory calculations.[37]

To provide a more quantitative and concise picture, we now focus on the vibrational state distribution of the H_2O product. In Figure 3, the H_2O vibrational state resolved and rotational state summed reaction probabilities are shown for the title reaction as a function of total energy. For the OH reactant in the ground vibrational state, the H_2O product is mostly found in the first stretching excited states, as shown in Figure 3a. The probabilities for forming the (100) and (001) states are similar in magnitude, especially at lower energies. The doubly excited (200), (101), and (002) states are also formed but with a higher threshold, and the (002) state has a much smaller probability than the other two. H_2O is also found to have some probabilities in its ground (000) and bending excited (010) vibrational states.

In contrast, the H_2O product is mostly found in the doubly excited anti-symmetric stretching state (002) if the OH reactant is in the first excited vibrational state, as shown in Figure 3b (note that its probability is scaled by a factor of 1/3 in the figure). The doubly excited symmetric stretching state (200) has a smaller probability and the probability of the combination stretching state (101) is even smaller. The singly excited states

DOI: 10.1021/jacs.5b11404
J. Am. Chem. Soc. 2015, 137, 15964−15970

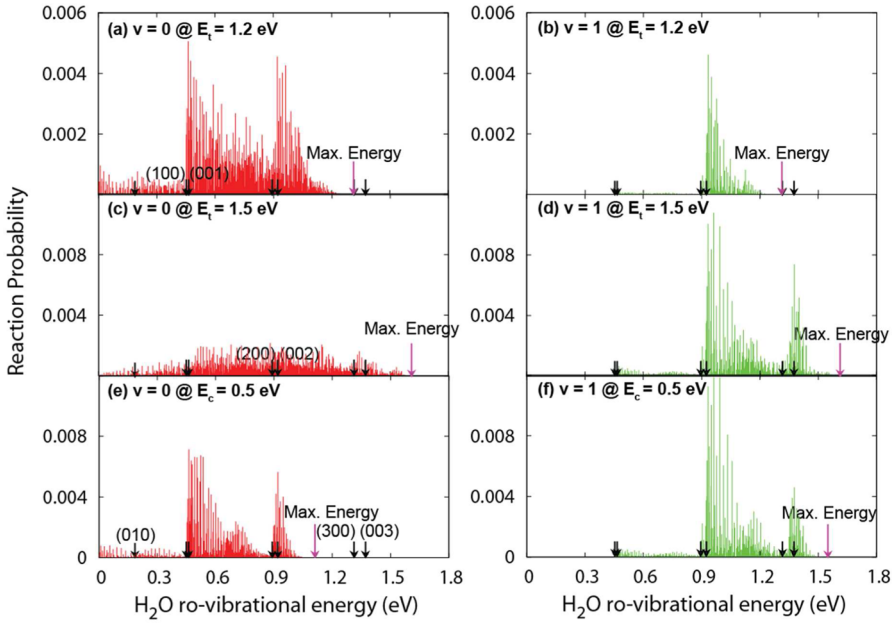

Figure 2. Final H_2O ro-vibrational state distributions for the reaction $H_2(v = 0, j = 0) + OH(v = 0,1, j = 0) \rightarrow H + H_2O$ at different energies. The distributions are plotted at two different total energies, (a,b) at E_t = 1.2 eV and (c,d) at E_t = 1.5 eV, and also at a collision energy E_c = 0.5 eV in (e,f). The energies of six excited stretching levels of the rotationless H_2O are marked by arrows, along with the maximally allowed energies ("Max. Energy").

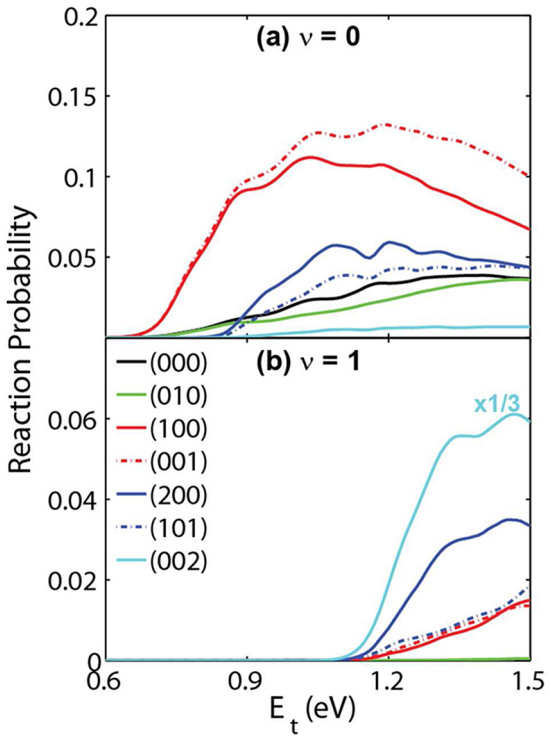

Figure 3. Final H_2O vibrational state resolved and rotational states summed state-to-state reaction probabilities in the reaction $H_2(v = 0, j = 0) + OH(v = 0,1, j = 0) \rightarrow H + H_2O(\nu_s\nu_b\nu_a)$ as a function of total energy: (a) the ground and (b) first excited OH reactant. The rotational states of each H_2O vibrational states are summed over.

(001) and (100) are also formed with smaller but nearly equal probabilities. Few H_2O is found in the ground and bending excited vibrational states. There is an overall ~0.44 eV energy shift in the energy threshold, compared with Figure 3a, which corresponds well to the vibrational excitation energy of OH reactant, again assignable to the spectator character of the OH moiety.

To better understand the drastically different populations of the H_2O vibrational states, the local-mode picture[44] is required, as it gives a better description of the stretching vibrations of this triatomic molecule. In this regime, the normal-mode wave functions ($|\nu_s\nu_b\nu_a\rangle$) can be written as linear combinations of the symmetrized local-mode counterparts ($|nm\rangle^{\pm}|\nu_b\rangle$), which are defined as follows:[44]

$$|(nm)^{\pm}\rangle = 1/\sqrt{2}\,(|nm\rangle \pm |mn\rangle), \quad n < m \tag{5a}$$

$$|(nm)^{\pm}\rangle = |nm\rangle, \quad n = m \tag{5b}$$

where $|nm\rangle$ denote the local-mode wave functions with n and m quanta in the two OH stretching modes, respectively. The leading local-mode terms and their weights are listed in Table 2

Table 2. Weights (%) of Symmetrized Local-Mode Bases in Several Low-Lying H_2O Normal-Mode Wavefunctions

	$\lvert C_{nm}\rvert^2$					
$(\nu_s\nu_b\nu_a)$	$\lvert(00)^+\rangle$	$\lvert(10)^+\rangle$	$\lvert(10)^-\rangle$	$\lvert(20)^+\rangle$	$\lvert(20)^-\rangle$	$\lvert(11)^+\rangle$
(000)	99.74	0.25				
(100)	0.76	98.28				
(001)		0.41	99.27			
(200)				76.82	4.94	15.83
(101)				3.48	93.12	1.57
(002)				18.11	0.13	81.17

for several low-lying H_2O normal-mode eigenstates. (The details of the local-mode calculations are given in Supporting Information.) This local-mode picture has been shown to provide a more in-depth characterization of mode specificity of the reverse $H + H_2O$ reaction.[38,45]

Without losing generality, we ignore the permutation symmetry between the two OH bonds in our discussion here.

DOI: 10.1021/jacs.5b11404
J. Am. Chem. Soc. 2015, 137, 15964−15970

This amounts to focusing on one of the two equivalent transition states. For the title reaction, it is thus important to note that the two local OH stretching modes of the H_2O product have different origins. One is newly formed through the reaction (denoted by n), while the spectator mode originated from the OH reactant (denoted by m). Due to the spectator nature of the latter, its excitation is expected to be largely determined by the excitation of the OH reactant, thanks to energy sequestration. On the other hand, the excitation of the former is due to energy flow from the reaction coordinate as the system moves from the transition state to the product asymptote.

In this local-mode representation, the H_2O product vibrational state distributions can now be readily understood. For the OH reactant in its ground vibrational state, only the newly formed OH bond can be excited, thanks to the spectator nature of the non-reactive OH moiety. As shown in Figure 3a, the H_2O product is mostly and equally produced at low energies in the (100) and (001) normal-mode states. According to Table 2, these normal-mode states correspond to one quantum in this newly formed OH mode, namely the $|10\rangle$ states. At higher energies, the (200) and (101) normal-mode states are also significantly populated. Table 2 further shows that these two states are dominated by the $|20\rangle$ local-mode states, indicating two quanta in the newly formed OH bond. The absence of excitation in the spectator OH bond again confirms the sequestration of the vibrational energy in the non-reactive OH mode.

For the OH reactant in its first excited vibrational state, on the other hand, the situation is quite different and more interesting. For the newly formed OH local mode in H_2O, it can be expected based on the aforementioned arguments that it will be dominated by one quantum excitation at low energies. In the meantime, the spectator OH mode is also expected to have one vibrational quantum due to energy sequestration in this moiety from the vibrationally excited OH reactant. Therefore, the most populated local-mode state at low energies would be $|11\rangle$, namely one quantum in each OH local mode. According to Table 2, this local-mode state has the largest weight in the (002) normal-mode state, followed by the (200) normal-mode state. This is borne out in Figure 3b, in which the (002) state has the dominant population followed by the (200) state. The (101) normal-mode state, which has the smallest weight of the $|11\rangle$ state, has expectedly the smallest population. It is clear that these observations are consistent with the conclusions of Crim and co-workers for the reactions involving highly excited H_2O.[26,27]

At this point, a natural question arises concerning the "loss of memory" effect discussed above, in which the product state distributions seemed to be independent of the reactant vibrational excitation.[19,23] To understand this dilemma, it is worth pointing out that these studies have all focused on excitations of *active* reactant modes, which are strongly coupled with the reaction coordinate at the transition state with large SVP values. For the $H/Cl + H_2O \rightarrow H_2/HCl + OH$ reactions, for example, the vibrational modes of H_2O all have significant projections on the reaction coordinate.[10] As a result, their excitations inevitably channel energy into the reaction coordinate,[11] and during this process their vibrational energies may be lost.[19,23] A recent work by Liu and Zhang offered an in-depth analysis of this phenomenon,[38] again using the local-mode picture. It was shown by these authors that for the $H + H_2O \rightarrow H_2 + OH$ reaction, the (100) and (001) normal-mode states of H_2O promote the reaction, but both lead to the OH product mostly in its ground vibrational state. As discussed above, these two normal-mode states are linear combinations of the $|10\rangle$ and $|01\rangle$ local-mode states. Those authors demonstrated that the cleaved OH bond is always the excited one. In both cases, the memory of the initial H_2O vibrational excitation is lost.

Interestingly, the two bonds in water can be distinguished if one of the hydrogens (H) is replaced by deuterium (D). Because the OH and OD modes are different, the local-mode picture becomes the canonical regime for describing the stretching vibration of HOD. As a result, the mode specificity manifests in the H + HOD reaction as bond selectivity. Crim, Zare, and their co-workers have indeed demonstrated that the excitation of either the OH or OD bond in HOD leads to the cleavage of the excited bond in the H + HOD reaction, and the corresponding diatomic product (OD or OH) also has little vibrational excitation.[26,27,46,47] These experimental observations have been reproduced by quantum reactive scattering calculations.[48]

The case discussed in the current work is however quite different, as the vibrational excitation is restricted to the *spectator* OH reactant. For a spectator mode, as alluded earlier, energy can scarcely flow into the reaction coordinate because of the weak coupling between them. The consequence is the sequestration of the internal energy. Indeed, the memory of the OH reactant vibrational excitation is thus kept in the vibrational state distribution of the H_2O product, as discussed above.

The picture that emerges from the above local-mode analysis is thus clear. The "loss of memory" effect only occurs when *active* reactant modes are excited, because of its facile energy flow into the reaction coordinate due to their strong couplings with the reaction coordinate. This effect is probably only prevalent near the reaction threshold though. On the other hand, energy is preserved in a *spectator* mode throughout the reaction because energy flow to the reaction coordinate is very inefficient. This key observation reveals whether and how the state-to-state mode specificity comes to existence in bimolecular reactions.

The final question is whether and how the transition state exercises any control of the energy sequestration. To answer this question, we rely again on the TSWP method, which is ideally suited for understanding the transition-state control of reactivity.[19,20,23] In this picture, the passage of the reaction flux from the reactant side to product side is gated by the thermal flux eigenstates. In Figure 4a,b, four final H_2O vibrational-state resolved and rotational-state-summed state-to-state reaction probabilities are plotted with respect to the number of thermal flux eigenpairs used in the calculation. With the increase of the number of thermal flux eigenpairs, all the state-to-state reaction probabilities gradually converge to the final values, confirming the convergence of the calculation.

The eigenfunctions of the thermal flux operator near the transition state can be assigned with the vibrational quantum number of the non-reactive OH moiety (n_{OH}). As shown in Figure 4c, the first few eigenstates are assignable to $n_{OH} = 0$, but those with $n_{OH} = 1$ start to appear after $n = 31$. It is worth noting that the state-to-state reaction probabilities from the vibrationally excited OH in Figure 4b feature multiple sharp steps, which are attributable to the thermal flux eigenstates with $n_{OH} = 1$. In comparison, the unexcited OH reactant does not require excitation of OH in the thermal flux eigenpairs to react, as shown in Figure 4a. This is another key finding of this work,

DOI: 10.1021/jacs.5b11404
J. Am. Chem. Soc. 2015, 137, 15964−15970

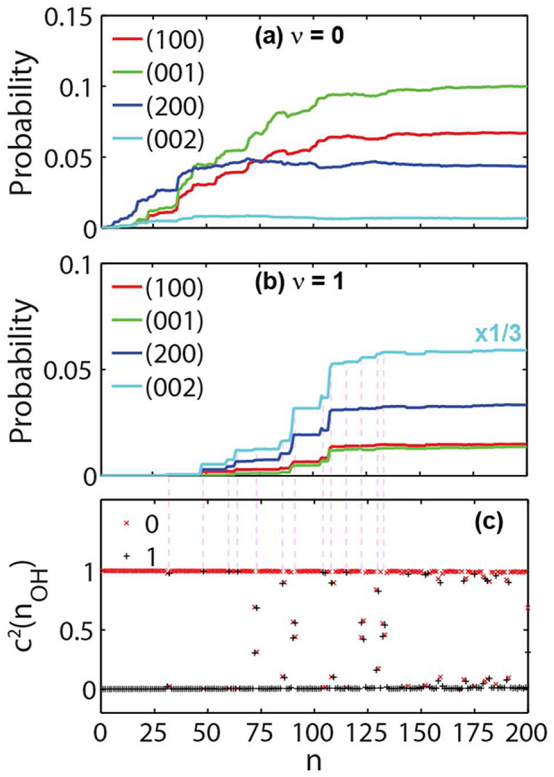

Figure 4. (a,b) Four final H_2O vibrational-state-resolved and rotational-state-summed state-to-state reaction probabilities of the reaction $H_2(\nu = 0, j = 0) + OH(\nu = 0,1, j = 0) \rightarrow H + H_2O(\nu_s\nu_b\nu_a)$ with respect to the number of thermal flux eigenpairs used in the calculation. The total energy is chosen at E_t = 1.5 eV. The OH reactant is in the (a) ground and (b) first excited vibrational states. (c) Fraction of OH vibrational states in the thermal flux eigenpairs.

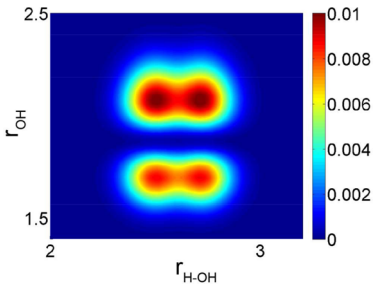

Figure 5. Squared wave function of the 32nd thermal flux eigenstate in the H + H_2O arrangement channel along the r_{H-OH} and r_{O-H} coordinates, while all other coordinates are integrated.

which suggests that the flow of energy sequestered in the OH moiety is gated by the transition state. Specifically in the TSWP model, the gating states are the thermal flux eigenstates with n_{OH} = 1. This is consistent with the higher reaction threshold for the excited OH reactant, shown in Figure 3b.

The wave function of a representative thermal flux eigenstate with n_{OH} = 1 is shown in Figure 5. The characteristic nodal structure in the non-reactive O−H coordinate is clearly visible. The node along H−OH coordinate is the feature of eigenstate of the thermal flux operator. It should be noted that thermal flux eigenstates are not energy eigenstates, but they do have relatively narrow energy spectra.[19] As a result, the reaction flux is not gated by a single thermal flux eigenpair, but by several acting in concert.[23] When a sufficient number of such eigenstates are involved, the gate for a particular reaction channel is open. In our case, the transfer of the sequestered vibrational energy in the OH spectator from the reactant side to product side is facilitated mainly by those gating states with n_{OH} = 1.

SUMMARY

Vibrational mode specificity in chemical reactions, namely the dependence of reactivity on reactant mode excitations, have helped to shed valuable light on reaction dynamics. In this publication, we focus on a more detailed issue in reaction dynamics, namely how reactant mode excitations shape up the product internal state distributions. Experimental evidence exists for both state-to-state mode specificity and the lack thereof, and a detailed theoretical investigation is thus needed to elucidate the quantum state resolved picture of energy flow during a chemical reaction.

To this end, we report full-dimensional state-to-state quantum scattering calculations for a prototypical four-atom bimolecular reaction, and analyze the energy flow from reactant side to the product side with full quantum resolution. It is shown that energy deposited into the reactant OH vibrational coordinate is sequestered during the reaction, and transferred into the H_2O stretching vibrational modes. As a result, the product internal state distribution depends strongly on the OH reactant vibrational excitation. A detailed analysis in the local-mode representation attributed the product vibrational excitations to different sources. While the spectator OH mode vibrational excitation in the H_2O product is directly from that of the OH reactant, the newly formed OH mode derives its excitation from energy flow along the reaction coordinate at the transition state. In addition, it is shown that this state-to-state mode specificity is not in conflict with the so-called "loss of memory" effect, in which the vibrational energy of an active reactant mode is lost because it flows readily into the reaction coordinate. Finally, it is shown that the transfer of sequestered internal energy is gated by the transition state via O−H vibrationally excited transition-state thermal flux eigenstates. This in-depth analysis sheds valuable light into the role of spectator modes in reactions involving large molecular systems and energy flow during a chemical process in general.

ASSOCIATED CONTENT

Supporting Information

The Supporting Information is available free of charge on the ACS Publications website at DOI: 10.1021/jacs.5b11404.

Theory, calculation details, and additional results (PDF)

AUTHOR INFORMATION

Corresponding Author

*hguo@unm.edu

Notes

The authors declare no competing financial interest.

ACKNOWLEDGMENTS

This material is based upon work supported by the U.S. Department of Energy, Office of Science, Office of Basic Energy Sciences, under Award No. DE-FG02-05ER15694 to H.G. Z.S. thanks National Natural Science Foundation of China (Grant No. 21222308).

DOI: 10.1021/jacs.5b11404
J. Am. Chem. Soc. 2015, 137, 15964−15970

REFERENCES

(1) Miller, W. H. *J. Phys. Chem. A* **1998**, *102*, 793.
(2) Fernandez-Ramos, A.; Miller, J. A.; Klippenstein, S. J.; Truhlar, D. G. *Chem. Rev.* **2006**, *106*, 4518.
(3) Yan, S.; Wu, Y.-T.; Liu, K. *Proc. Natl. Acad. Sci. U. S. A.* **2008**, *105*, 12667.
(4) Crim, F. F. *Acc. Chem. Res.* **1999**, *32*, 877.
(5) Crim, F. F. *Proc. Natl. Acad. Sci. U. S. A.* **2008**, *105*, 12654.
(6) Liu, K. *J. Chem. Phys.* **2015**, *142*, 080901.
(7) Li, J.; Jiang, B.; Song, H.; Ma, J.; Zhao, B.; Dawes, R.; Guo, H. *J. Phys. Chem. A* **2015**, *119*, 4667.
(8) Polanyi, J. C. *Acc. Chem. Res.* **1972**, *5*, 161.
(9) Jiang, B.; Guo, H. *J. Chem. Phys.* **2013**, *138*, 234104.
(10) Jiang, B.; Guo, H. *J. Am. Chem. Soc.* **2013**, *135*, 15251.
(11) Guo, H.; Jiang, B. *Acc. Chem. Res.* **2014**, *47*, 3679.
(12) Schatz, G. C.; Ross, J. *J. Chem. Phys.* **1977**, *66*, 1021.
(13) Gustafsson, M.; Skodje, R. T. *J. Chem. Phys.* **2006**, *124*, 144311.
(14) Welsch, R.; Manthe, U. *J. Chem. Phys.* **2014**, *141*, 051102.
(15) Welsch, R.; Huarte-Larrañaga, F.; Manthe, U. *J. Chem. Phys.* **2012**, *136*, 064117.
(16) Manthe, U.; Welsch, R. *J. Chem. Phys.* **2014**, *140*, 244113.
(17) Miller, W. H. *J. Chem. Phys.* **1974**, *61*, 1823.
(18) Miller, W. H.; Schwartz, S. D.; Tromp, J. W. *J. Chem. Phys.* **1983**, *79*, 4889.
(19) Welsch, R.; Manthe, U. *Mol. Phys.* **2012**, *110*, 703.
(20) Welsch, R.; Manthe, U. *J. Phys. Chem. Lett.* **2015**, *6*, 338.
(21) Zhao, B.; Sun, Z.; Guo, H. *J. Chem. Phys.* **2014**, *140*, 234110.
(22) Zhao, B.; Sun, Z.; Guo, H. *J. Chem. Phys.* **2014**, *141*, 154112.
(23) Zhao, B.; Guo, H. *J. Phys. Chem. Lett.* **2015**, *6*, 676.
(24) Zhao, B.; Sun, Z.; Guo, H. *J. Chem. Phys.* **2015**, *142*, 241101.
(25) Bronikowski, M. J.; Simpson, W. R.; Zare, R. N. *J. Phys. Chem.* **1993**, *97*, 2204.
(26) Sinha, A.; Hsiao, M. C.; Crim, F. F. *J. Chem. Phys.* **1991**, *94*, 4928.
(27) Sinha, A.; Thoemke, J. D.; Crim, F. F. *J. Chem. Phys.* **1992**, *96*, 372.
(28) Zhang, D. H.; Light, J. C. *J. Chem. Phys.* **1996**, *105*, 1291.
(29) Zhu, W.; Zhang, J. Z. H.; Zhang, D. H. *J. Chem. Phys.* **1996**, *105*, 4881.
(30) Strazisar, B. R.; Lin, C.; Davis, H. F. *Science* **2000**, *290*, 958.
(31) Zhang, D. H.; Xie, D.; Yang, M. *Phys. Rev. Lett.* **2002**, *89*, 283203.
(32) Brouard, M.; Burak, I.; Marinakis, S.; Minayev, D.; O'Keeffe, P.; Vallance, C.; Aoiz, F. J.; Banares, L.; Castillo, J. F.; Zhang, D. H.; Xie, D.; Yang, M.; Lee, S.-Y.; Collins, M. A. *Phys. Rev. Lett.* **2003**, *90*, 093201.
(33) Zhang, D. H. *J. Chem. Phys.* **2006**, *125*, 133102.
(34) Xiao, C.; Xu, X.; Liu, S.; Wang, T.; Dong, W.; Yang, T.; Sun, Z.; Dai, D.; Xu, X.; Zhang, D. H.; Yang, X. *Science* **2011**, *333*, 440.
(35) Cvitaš, M. T.; Althorpe, S. C. *J. Chem. Phys.* **2013**, *139*, 064307.
(36) Smith, I. W. M.; Crim, F. F. *Phys. Chem. Chem. Phys.* **2002**, *4*, 3543.
(37) Li, J.; Corchado, J. C.; Espinosa-García, J.; Guo, H. *J. Chem. Phys.* **2015**, *142*, 084314.
(38) Liu, S.; Zhang, D. H. *Chem. Sci.* **2015**, DOI: 10.1039/C5SC03472H.
(39) Matzkies, F.; Manthe, U. *J. Chem. Phys.* **1997**, *106*, 2646.
(40) Manthe, U. *J. Chem. Phys.* **1995**, *102*, 9205.
(41) Yang, M.; Zhang, D. H.; Collins, M. A.; Lee, S.-Y. *J. Chem. Phys.* **2001**, *115*, 174.
(42) Zhang, D. H.; Yang, M.; Lee, S.-Y. *J. Chem. Phys.* **2001**, *114*, 8733.
(43) Zhang, D. H.; Yang, M.; Lee, S.-Y. *J. Chem. Phys.* **2002**, *116*, 2388.
(44) Child, M. S.; Halonen, L. *Adv. Chem. Phys.* **1984**, *57*, 1.
(45) Fu, B.; Zhang, D. H. *J. Chem. Phys.* **2013**, *138*, 184308.
(46) Bronikowski, M. J.; Simpson, W. R.; Girard, B.; Zare, R. N. *J. Chem. Phys.* **1991**, *95*, 8647.
(47) Bronikowski, M. J.; Simpson, W. R.; Zare, R. N. *J. Phys. Chem.* **1993**, *97*, 2194.
(48) Fu, B.; Zhang, D. H. *J. Chem. Phys.* **2015**, *142*, 064314.

DOI: 10.1021/jacs.5b11404
J. Am. Chem. Soc. 2015, 137, 15964−15970